Novel Guest−Host NLO Poly(ether imide) Based on a Two-Dimensional Carbazole Chromophore with Sulfonyl Acceptors

Wen-Jang Kuo,[†] Ging-Ho Hsiue,*[,†,‡] and Ru-Jong Jeng[‡]

Department of Chemical Engineering, National Tsing Hua University, Hsinchu, Taiwan, 300, ROC; and Department of Chemical Engineering, National Chung Hsing University, Taichung, Taiwan, 402, ROC

Received October 10, 2000; Revised Manuscript Received January 16, 2001

ABSTRACT: Taking advantage of the multifunctional characteristics of carbazole along with rational molecular design, a two-dimensional (2-D) carbazole chromophore was synthesized by a facile synthetic route. By doping of the chromophores into an organosoluble poly(ether imide), a series of guest−host NLO polymers were acquired. A high doping level up to 38 wt % was obtained without observing aggregation of NLO chromophores. The second harmonic coefficients (d_{33}) for the guest−host system range from 5 to 22 pm/V, dependent on the doping level. The compatibility between chromophore and poly(ether imide) was investigated by SEM and extraction experiment. In the aspect of compatibility, the molecular weight distribution of the polymer plays an important role. The effect of two-dimensional structure on the NLO temporal stability was investigated by tracing the second harmonic coefficient as functions of temperature and time, respectively. Moreover, the relaxation behavior of the NLO systems was further examined by dielectric analysis. Large rotational cone volumes give the two-dimensional chromophore excellent orientational stability when the temperature approaches the glass transition temperature observed from DEA.

Introduction

Second-order nonlinear optical (NLO) materials have attracted interest because of their potential applications in optoelectronic technology.[1−3] These NLO polymers could be acquired via doping NLO chromophores into amorphous polymer matrices (guest−host systems)[4] or covalently incorporating NLO moieties onto polymer backbone.[5−7] Most of attempted chromophores are designed as one-dimensional "push−pull" compounds. Such chromophores are represented as D−π−A, where the electron-donor (D) and electron-acceptor (A) groups are linked by a π-conjugated bridge.[8,9] These chromophores exhibit large first-order hypersusceptibility, β. However, the one-dimensional compounds provide less phase-matching behavior owing to their small off-diagonal component.[10,11] Two-dimensional (2-D) chromophores have been observed, possessing better phase-matching than one-dimensional chromophores because of their larger off-diagonal components.[12] These chromophores provide not only a better phase-matching capacity but also an asymmetric arrangement.

In this work, carbazole derivatives were chosen as NLO chromophores because of their multifunctional properties, such as second-order NLO and photorefractive properties.[13−16] Furthermore, 2-D chromophores can be synthesized in the carbazole derivatives because of their isoelectronic structures between the 3 and 6 positions. The 2-D chromophores provide some unique second-order NLO properties,[17−19] such as a large off-diagonal tensor component, and excellent temporal stability.

Guest−host NLO systems are highly accessible for studying the macroscopic NLO properties of the polymers despite of limited miscibility between chromophores and polymers.[20−23] Moreover, the issue of enhancing compatibility between chromophore and polymer matrix also has been investigated in the systems. Aromatic polyimides are excellent candidates for NLO applications because of their robust mechanical properties and high thermal and chemical resistance. For NLO polyimides, NLO poly(amic acid)s were used as the precursor owing to their poor solubility. However, the polyimides were somewhat restricted for guest−host NLO systems because of sublimation and decomposition of the chromophores during imidization process. To circumvent imidization process, utilization of organosoluble polyimides seems to be a reasonable approach. Disrupting symmetry and regularity of the polymer backbone is a major method used for improving the solubility while maintaining the high temperature performance of polyimides.[24−30] Structural modification to improve solubility includes incorporation of flexible bridging linkage,[24−28] meta-oriented or ortho-oriented phenylene rings,[29,30] and aromatic ether linkages into aromatic polymer backbone.

In this work, a two-dimensional chromophore based on carbazole derivatives was synthesized. An organosoluble poly(ether imide), 6FPEI, based on bis(aminophenoxy)biphenyl was served as the polymeric matrices for the NLO chromophores. Guest−host NLO systems were acquired by doping the chromophores into the poly(ether imide) with various contents. A systematic investigation of variation of the chromophore contents on NLO properties has been pursued. The correlation between structure and nonlinear optical characteristics was investigated by thermal dynamic and temporal relaxation behaviors and dielectric analysis. The compatibility between chromophores and polymer matrix was also studied by SEM and extraction experiment.

* To whom correspondence should be addressed. E-mail: ghhsiue@che.nthu.edu.tw. Fax: 886-3-5726-825.
[†] National Tsing Hua University.
[‡] National Chung Hsing University.

10.1021/ma0017485 CCC: $20.00
Published on Web 02/24/2001

Experimental Section

Materials. Chemicals such as carbazole, $POCl_3$, 1-bromohexane, triethyl phosphite, *p*-thiocresol, *N*-bromosuccinimide, 2,2′-biphenol, and hydrazine monohydrate were purchased from Lancaster, ACROS, STREM Chemicals, and TCI. They are used as received. Solvents such as NMP, DMAc, DMF, THF, and dichloromethane were purchased from TEDIA. NMP, DMAc, and DMF were dried over calcium hydride and distilled under vacuum. THF was dried over sodium and distilled.

Synthesis of the NLO Chromophore. 9-Hexyl Carbazole. The solution of carbazole (20 g; 120 mmol) in dry DMAc (50 mL) was added dropwise to the suspended sodium hydride (5.8 g 60 wt % in mineral oil; 145 mmol) in dry DMAc (50 mL) under nitrogen atmosphere at 0 °C for a period of 30 min. After addition of 1-bromohexane (30 g; 180 mmol), the solution was stirred for 6 h at room temperature. Deionic water was added to terminate sodium hydride, and the solution was extracted with ethyl acetate several times. After the extract was washed with deionic water, the extract was concentrated. Further purification was performed with column chromatography (pure normal hexane as eluent). ^{1}H NMR ($CDCl_3$): δ = 0.83−0.87 (t, 3H, −C*H*$_3$), 1.25−1.40 (m, 6H, −C*H*$_2$−), 1.82−1.88 (p, 2H, −N−CH$_2$−C*H*$_2$−), 4.26−4.30 (t, 2H, −N−C*H*$_2$−), 7.20−7.24 (t, 2H, Ar−*H*, para to NH), 7.38−7.41 (d, 2H, Ar−*H*, ortho to NH), 7.43−7.47 (t, 2H, Ar−*H*, meta to NH), 8.08−8.10 (d, 2H, Ar−H, ortho to NH). Anal. Calcd for $C_{18}H_{21}N$: C, 86.01; H, 8.42; N, 5.57. Found: C, 86.12; H, 8.31; N, 5.54.

9-Hexyl-9*H*-3,6-Diformyl Carbazole. DMF (30 g) was added dropwise to $POCl_3$ solution under 0 °C. After addition of the solution of 9-hexyl carbazole in 1,2-dichloroethane (50 mL), the reaction mixture was heated to 100 °C and kept stirring at this temperature for 24 h. When the reaction was completed, the reaction solution was added to cool NaOH aqueous solution (5%) and then extracted with dichloromethane for several times. The organic layer was separated, washed with deionic water three times, dried over anhydrous magnesium sulfate, and condensed with aspirator. Further purification was performed by column chromatography using dichloromethane/hexane 2/3 as eluent. Mp: 131 °C. ^{1}H NMR ($CDCl_3$): δ = 0.76−0.80 (t, 3H, −C*H*$_3$), 1.17−1.32 (m, 6H, −C*H*$_2$−), 1.80−1.84 (p, 2H, N−CH$_2$−C*H*$_2$−), 4.27−4.30 (t, 2H, −C*H*$_2$−), 7.44−7.46 (d, 2H, Ar−*H*, ortho to NH), 7.98−8.00 (d, 2H, Ar−*H*, ortho to CHO), 8.55 (s, 2H, Ar−*H*, ortho to CHO), 10.04 (s, 2H, C*H*O). Anal. Calcd for $C_{20}H_{21}NO_2$: C, 78.15; H, 6.89; N, 4.56. Found: C, 78.08; H, 6.83; N, 4.51.

Ethyl (4-Methylphenyl) Sulfide. To a solution of *p*-thiocresol (5.3 g, 43 mmol) in dry DMF (30 mL) was added potassium carbonate (7.1 g, 52 mmol) under nitrogen atmosphere at room temperature for a period of 30 min. After addition of bromoethane (5.6 g, 52 mmol), the reaction mixture was stirred for 24 h at 50 °C. The solution was then poured over deionic water, and the resulting mixture was extracted with ethyl acetate three times. After the organic extracts were washed with deionic water, the organic layer was dried over anhydrous magnesium sulfate and condensed. Further purification was performed with column chromatograph to produce transparent liquid. Yield: 5.9 g, 91%. ^{1}H NMR ($CDCl_3$): δ 1.30 (t, 3H, −C*H*$_3$), 2.33 (s, 3H, Ph−C*H*$_3$), 2.91 (q, 2H, S−C*H*$_2$−), 7.10 (d, 2H, Ar−H, ortho to SCH$_2$−), 7.26 (d, 2H, Ar−H, ortho to CH$_3$). Anal. Calcd for $C_9H_{12}S$: C, 71.00; H, 7.94; S, 21.06. Found: C, 70.92; H, 7.85; S, 21.23.

4-(Ethylsulfonyl)toluene. To a solution of 4-methylphenyl ethyl sulfide (10.2 g, 38 mmol) in glacial acetic acid (20 mL) was added hydrogen peroxide (10.8 g, 30% solution). The resulting mixture was refluxed for 5 h and then concentrated by reduced distillation. The residue was dissolved in ethyl acetate and washed with deionic water. The organic layer was condensed after drying over anhydride magnesium sulfate. Further purification was performed with column chromatography to produce a viscous liquid. Yield: 92%. ^{1}H NMR ($CDCl_3$): δ 1.22−1.25 (t, 3H, −C*H*$_3$), 2.42 (s, 3H, Ph−C*H*$_3$), 2.98 (q, 2H, SO$_2$−C*H*$_2$−), 7.32 (d, 2H, Ar−H, meta to SO$_2$-), 7.75 (d, 2H, Ar−H, ortho to CH$_3$). Anal. Calcd for $C_9H_{12}O_2S$: C, 58.67; H, 6.56; S, 17.4. Found: C, 58.56; H, 6.49; S, 17.61.

4-(Ethyl sulfonyl)benzyl Bromide. 4-(Ethylsulfonyl)-toluene (2.0 g, 6.7 mmol), *N*-bromosuccinimide (1.3 g, 7.4 mmol), and benzoyl peroxide (0.015 g) were dissolved in 20 mL of CCl_4. The resulting solution was refluxed under a nitrogen atmosphere for 12 h. The mixture solution was cooled and washed with deionic water. The organic layer was concentrated after drying over anhydride magnesium sulfate. The product was obtained by recrystallization from ethyl acetate and hexane solution. Yield: 83%. ^{1}H NMR ($CDCl_3$): δ 1.26 (t, 3H,SO$_2$−CH$_2$−C*H*$_3$), 3.09 (q, 2H, SO$_2$−C*H*$_2$−), 4.49 (s, 2H, Ph−C*H*$_2$Br), 7.56 (d, 2H, Ar−H, meta to SO$_2$−), 7.85 (d, 2H, Ar−H, ortho to SO$_2$). Anal. Calcd for $C_9H_{11}BrO_2S$: C, 41.08; H, 4.21; Br, 30.36; S, 12.18. Found: C, 40.96; H, 4.23; Br, 30.28; S, 12.26.

Diethyl [4-(Ethylsulfonyl)benzyl] Phosphate. 4-(Ethylsulfonyl)benzyl bromide (2.9 g, 7.8 mmol) was dissolved in 15 mL of dry triethyl phosphite. The mixture solution was stirred and refluxed for 6 h. Excessive triethyl phosphite was distilled away when the reaction was completed. The residue was redissolved with ethyl acetate, and washed with deionic water. The organic layer was condensed after drying over anhydrous magnesium sulfate. Further purification was performed by column chromatograph. Yield: 2.82 g, 83%. ^{1}H NMR ($CDCl_3$): δ 1.07 (t, 9H, P−OCH$_2$−C*H*$_3$, and −SO$_2$CH$_2$C*H*$_3$), 2.93 (q, 2H, −SO$_2$−C*H*$_2$−), 3.06 (d, 2H, Ph−C*H*$_2$−P(O)(OEt)$_2$, J = 22.5 Hz), 3. 89 (t, 4H, −P(O)−(OC*H*$_2$−Me)$_2$), 7.34 (d, 2H, Ar−H, meta to −SO$_2$−), 7.85 (d, 2H, Ar−H, ortho to −SO$_2$−). ^{31}P NMR δ = 24.56 ppm. Anal. Calcd for $C_{13}H_{21}O_5PS$: C, 48.74; H, 6.61; P, 9.67; S, 10.01. Found: C, 48.63; H, 6.58; P, 9.73; S, 10.12.

3,6-Di(2′-(4″-ethxylsulfonylphenyl)-1′-ethenyl)-9-hexyl 9*H*-Carbazole (Cz2PhSO$_2$). To a suspension solution of sodium hydride (NaH, (0.32 g, 60% in mineral oil, 13.5 mmol) in dry tetrahydrofuran (THF, 5 mL) was added a mixed solution of 9-hexyl-9*H*-3,6-diformyl carbazole (0.5 g, 1.63 mmol) and 4-(ethyl sulfonyl)benzyl diethyl phosphate (2.34 g, 5.4 mmol) in dry THF (5 mL) dropwise under nitrogen atmosphere at 0 °C. After the reaction was stirred at 0 °C for 4 h, deionic water (20 mL) was added to terminate the reaction which was condensed with an aspirator. The crude product was further purified by flash chromatography. Yield: 89%. ^{1}H NMR ($CDCl_3$): δ 0.83 (t, 3H, −C*H*$_3$), 1.23−1.37 (m, 12H, −CH$_2$−), 1.86 (m, 2H, N−CH$_2$C*H*$_2$−), 3.12 (q, 4H, SO$_2$−C*H*$_2$−), 4.29 (t, 2H, −N−C*H*$_2$−), 7.15 (d, 2H, CH=C*H*-PhSO$_2$−, J = 16 Hz), 7.39 (d, 4H, Ar−H, meta to vinyl group), 7.45 (d, 2H, C*H* = CH−PhSO$_2$−, J = 16 Hz), 7.69 (d, 6H, Ar−H, meta to SO$_2$− and ortho to vinyl group), 7.87 (d, 4H, Ar−H, ortho to SO$_2$−), 8.27 (s, 2H, Ar−H, ortho to vinyl group). Anal. Calcd for $C_{38}H_{41}NO_4S_2$: C, 71.33; H, 6.46; N, 2.19; S, 10.02. Found: C, 71.52; H, 6.21; N, 2.15; S, 10.12.

1,1′-Bis(*p*-nitrophenoxy)-2,2′-biphenyl. To a solution of 2,2′-biphenol (20 g, 107 mmol) in dried DMF (100 mL) was added sodium carbonate (37 g, 0.35 mol) under nitrogen atmosphere. After this was stirred at room temperature for 30 min, *p*-fluoronitrobenzene (33 g, 0.234 mol) was added. The solution was kept at 80 °C for 6 h. After the solution was poured into deionic water, the suspension solution was filtered and washed with deionic water. Further purification was performed by recrystallization from EA. Yield: 83%. ^{1}H NMR ($CDCl_3$): δ 6.68 (d, 4H, Ar−*H*, meta to nitro group), 7.13 (d, 2H, Ar−H, ortho to ether group), 7.29 (t, 2H, Ar−*H*, para to ether group), 7.43 (t, 4H, Ar−*H*, meta to ether group), 8.09 (t, 4H, Ar−*H*, ortho to nitro group). Anal. Calcd for $C_{24}H_{16}N_2O_6$: C, 67.29; H, 3.76; N, 6.54. Found: C, 67.52; H, 3.82; N, 6.22.

1,1′-Bis(*p*-aminophenoxy)-2,2′-biphenyl. (4,4′-Dinitrophenyl)-2,2′-biphenyl (5.06 g, 14 mmol) and Pd/C (0.07 g of 10% Pd in active carbon) were added to ethanol (50 mL). The suspension solution was heated to 80 °C. Hydrazine monohydrate (18 mL) was added to the solution dropwise. The solution was stirred at this temperature for 6 h. Ethanol and excessive hydrazine monohydrate was removed by reduced pressure distillation. Further purification was performed using column chromatography. A white crystal was obtained. Yield: 87%. ^{1}H

NMR ($CDCl_3$): δ 4.90 (s, 4H, Ar−N*H*$_2$), 6.46 (d, 4H, Ar−*H*, meta to amino group), 6.63 (t, 6H, Ar−*H*, ortho to amino group and meta to ether group), 7.03 (t, 2H, Ar−H, para to ether group), 7.20 (t, 2H, Ar−*H*, meta to ether group), 7.32 (d, 2H, Ar−*H*, otho to ether group). Anal. Calcd for $C_{24}H_{20}N_2O_2$: C, 78.24; H, 5.47; N, 7.60. Found: C, 78.28; H, 5.39; N, 7.32.

Polyimide. After (4,4′-diaminophenyl)-2,2′-biphenyl (4.11 g, 11 mmol) was dissolved into a dried NMP solution (15 mL) at 0 °C, dianhydride, 6FDA (4.96 g, 11 mmol) was slowly added to the solution. The solution was stirred at room temperature for 2 h. Adding the solution to methanol solution dropwise, the polyamic acid was precipitated. The precipitate was washed with methanol and dried over reduced pressure. Thermal imidization was performed at 250 °C for 30 min. Yield: 93%. T_g = 220 °C; T_d = 499 °C. Anal. Calcd for $C_{43}H_{22}F_6N_2O_6$: C, 66.50; H, 2.85; F, 14.68; N, 3.61. Found: C, 66.07; H, 2.92; F, 14.22; N, 3.52.

Characterization. Chemical structures were identified by Fourier transform infrared spectra (FT-IR) and ^{1}H NMR spectra. FT-IR spectra were measured with a Bio-Rad FT-IR spectrometer and were performed by mixing samples with KBr powder and pressing the mixture into pellets. ^{1}H NMR spectra were recorded with the use of a INOVA-500 spectrometer, and chemical shifts are reported in ppm units. Thermal transition behaviors were determined by a Seiko SSC/5200 differential scanning calorimeter (DSC) at a heating rate of 10 °C/min. Thermal degradation temperatures of these compounds were measured by a Seiko 2200 thermogravimetric analyzer (TGA) at a heating rate of 10 °C/min under nitrogen atmosphere. Linear optical properties were measured with a Perkin-Elmer Lambda UV−vis spectra.

Thin Film Preparation. Various ratios of poly(ether imide) and chromophore $Cz2PhSO_2$ were dissolved in spectroscopic grade *N*-methylpyrrolidone (NMP). The solution concentrations were controlled to be about 20 wt %. The solutions were filtered by a 0.22 μm microsyringe. High-quality polymer films were obtained by spin-coating the solution onto indium tin oxide (ITO) coated glass substrates. The spin-coated film was dried at 50 °C for 30 min and then under vacuum at 100 °C overnight.

Simultaneous in Situ Poling and Curing. A corona poling process for the polymer films was carried out using the in situ poling technique. The corona discharge was generated from a tungsten wire, which was placed parallel across a 1.0 cm gap above the polymer film. The corona field of 7 kV was applied after the film was heated to 100 °C. The temperature was slowly elevated to 150 °C and then kept at this temperature for 20 min. Finally, temperature was slowly cooled to room temperature. During poling, the corona current was maintained at 1−2 μA.

Nonlinear Optical Properties Measurement. Second harmonic (SH) coefficients (d_{33}) of the poled films were measured by a Q-switched Nd:YAG laser at 1.064 μm. An Y-cut quartz crystal (d_{11} = 0.5 pm/V) was used as reference. A Metricon 2010 Prism Coupler measured refractive indices and thickness of the polymer films. Relaxation behaviors were investigated by monitoring the decay of the effective SH coefficient, d_{eff}, as a function of time at various temperatures.

Morphology Studies. The morphology of the fractured surfaces of the guest−host NLO systems was characterized by a Hitachi S-4700I high-resolution scanning electron microscope (SEM) and extraction experiment. The polymer solutions were prepared in the same manner as for spin coating. The solutions were cast onto glass cells and dried at 80 °C for 3 days. Cast films can be treated with or without cosolvent of acetonitrile and methanol (ratio 2:1). The joint study of extraction and SEM is essential in determining dispersion of the chromophores in polymer matrices.

Dielectric Analysis. Dielectric relaxation behavior of the NLO guest−host systems was investigated by dielectric spectroscopy using a Novercontrol GmbH equipped Schlumberger SI 1260 impedance and gain-phase analyzer as well as a Quator temperature controller. The polymer solutions were prepared in the same manner as for spin-coating. The solutions were cast onto the DEA cells and dried at 80 °C for 3 days. The measured temperature were controlled between −100 and +200 °C. The frequencies scanned ranged from 100 mHz to 1 MHz.

Scheme 1. Synthesis of the Carbazole-Containing NLO Chromophore $Cz2PhSO_2$

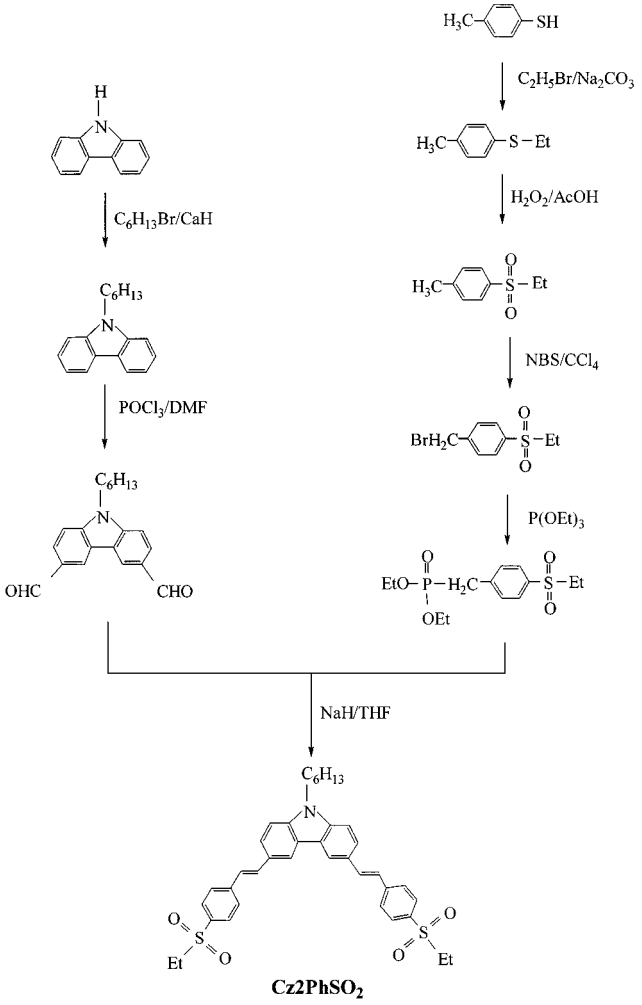

Result and Discussion

Synthesis and Identification of the Carbazole-Containing Chromophore. A new chromophore containing carbazole, $Cz2PhSO_2$ has been synthesized via the Knoevenagel condensation reaction. Scheme 1 depicts the synthetic route of the chromophore. In the scheme, a diformyl carbazole was obtained first. After condensing the diformyl carbazole with diethyl (4′-ethylsulfonylbenzyl) phosphonate, a two-dimensional chromophore $Cz2PhSO_2$ was obtained. Figure 1 shows the FT-IR of the chromophore $Cz2PhSO_2$. The asymmetric and symmetric stretching bands of sulfonyl groups appear at 1312 and 1146 cm^{-1}, respectively. The characteristic stretching band of the conjugated vinyl group appears at 1625 cm^{-1}.

Figure 2 shows the ^{1}H NMR of the carbazole-containing chromophore $Cz2PhSO_2$ in chloroform-*d*. In the spectrum, the chemical shifts of the vinyl protons appeared at 7.15 ppm with a coupling constant of 16 Hz and at 7.45 ppm with a coupling constant of 16 Hz. The chemical shifts of the aromatic protons in the sulfonyl phenyl group appeared at 7.87 and 7.70 ppm, respectively. Other chemical shifts of the aromatic protons in carbazole are assigned in the spectrum.

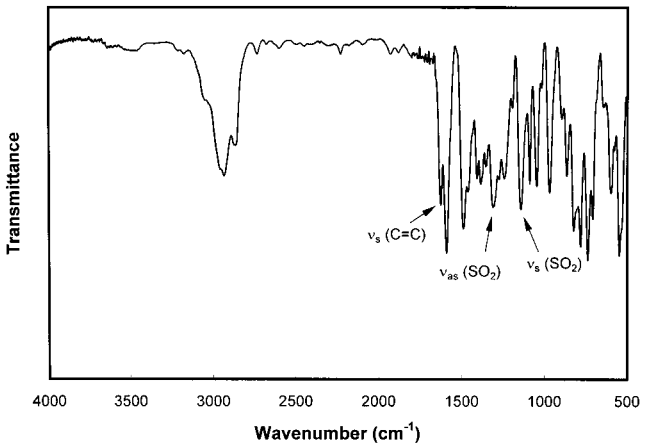

Figure 1. FT-IR spectrum of the chromophore Cz2PhSO$_2$.

Thermal properties of the chromophore Cz2PhSO$_2$ were characterized by DSC and TGA at a heating rate of 10 °C/min under nitrogen atmosphere. A degradation temperature (T_d; 5 wt % weight loss) was observed at 388 °C in TGA thermogram. The T_d value is similar to that observed in DSC thermogram. This high T_d chromophore is more stable than commercially available NLO dyes, such as DO3 (T_d = 235 °C), and DR19 (T_d = 260 °C).[31] Moreover, a melting point (T_m) was found at 183 °C in DSC thermogram for the chromophore Cz2PhSO$_2$.

Identification and Thermal Properties of Poly(ether imide). Scheme 2 depicts the synthesis route of the organosoluble poly(ether imide). In the scheme, an aromatic diamine was acquired first. By condensing the diamine with dianhydride 6FDA, a polyamic acid was obtained. The organosoluble poly(ether imide) was

Scheme 2. Synthesis of the Organosoluble Poly(ether imide) 6FPEI

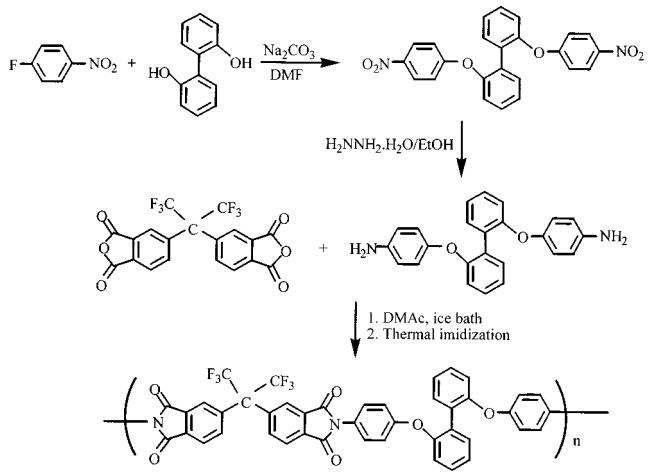

obtained via thermal imidization at 250 °C for 30 min. The poly(ether imide) possesses excellent solubility in common organic solvents such as NMP, DMF, DMSO, cyclohexanone, THF, and chloroform. Molecular weight was determined by Waters GPC-150 using DMF as eluent, and monodispersed polystyrenes as standard. An M_w of 38 000 with a polydispersity index of 1.8 was observed.

Figure 3 shows FT-IR spectrum for the poly(ether imide) 6FPEI. The asymmetric and symmetric stretching bands of imide groups appear at 1787 and 1730 cm^{-1}, respectively. Figure 4 shows the ^{1}H NMR spectrum of the poly(ether imide) 6FPEI. Chemical shifts of the aromatic protons of dianhydride appeared at 7.69, 7.87, and 8.07 ppm, whereas chemical shifts contributed from diamine appeared between 6.90 and 7.45 ppm.

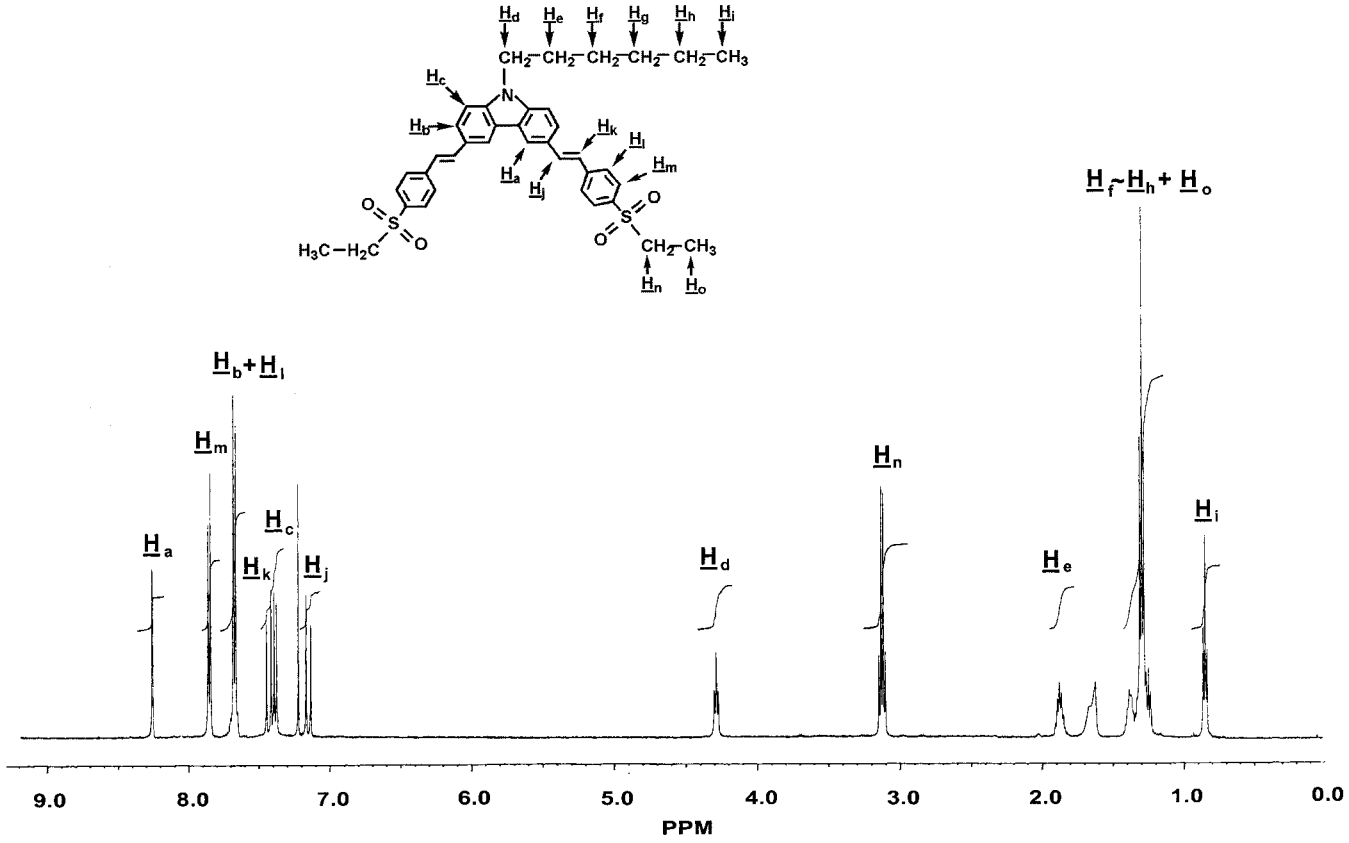

Figure 2. ^{1}H NMR spectrum of the chromophore Cz2PhSO$_2$.

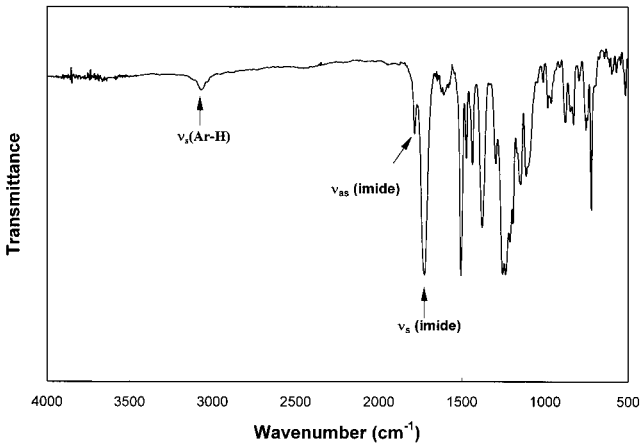

Figure 3. FT-IR spectrum of the soluble poly(ether imide) 6FPEI.

Figure 5 shows DSC and TGA thermograms of the pristine poly(ether imide). T_g and T_d were observed at 220 and 499 °C, respectively. Excellent thermal stability makes this poly(ether imide) suitable as polymer host for NLO chromophores.

Thermal Properties of the Guest−Host NLO Poly(ether imide)s. Chromophore contents in the poly(ether imide)s were 0.3, 0.4, 0.5, and 0.6 mmol in 1 g of polymer host for PICz3m, PICz4m, PICz5m, and PICz6m, respectively. The NLO-active poly(ether imide)s were dissolved in NMP, and the concentration was controlled at 20% w/v. Excellent quality films were obtained by spin-coating the solution onto ITO glass substrates. No macroscopic phase separation was found in the guest−host systems despite that the doping level was as high as 38 wt %. It is important to note that such high doping level is extraordinary as compared to other guest−host NLO systems.[32,33] This implies that excellent compatibility between poly(ether imide) and chromophore was obtained in the guest−host systems.

Figure 6 show the DSC thermograms of the guest−host NLO poly(ether imide)s. In DSC thermogram, transition behavior were observed between 50 and 100 °C. The transition temperature almost remained constant and decreased as the chromophore content increased. The transition behavior would be identified to be the local motion of the biphenoxy group of the polymer backbone by DEA analysis. Moreover, the intensity of the transition increased as the chromophore contents increased. This implies that plasticizer effect was present in the NLO-active guest−host polymers. The doped chromophores enlarge the free volume of the poly(ether imide). This makes the biphenoxy group in the NLO-active polymer more mobile than that in the pristine polymer. Furthermore, two endothermic peaks were found in the thermograms. These endothermic peaks may be possibly caused by macroscopic phase separation or sublimation of the chromophore Cz2PhSO$_2$. Several techniques were applied to characterize the endothermic peaks and the transition behavior. These include TGA thermogram, dielectric analysis, and absorption spectrum under various thermal treatments.

Figure 7 shows the TGA thermograms of the NLO-active poly(ether imide)s. Three stages of thermal degradation were found. As compared with the pristine poly(ether imide) and chromophore Cz2PhSO$_2$, the first-stage degradation (160 °C) of the guest−host system may be contributed from sublimation of the chromophore. This sublimation of the chromophore in polymer matrices was identified by detecting UV−vis absorbances at various annealing conditions, which will be discussed in the Optimization of the Poling Condition

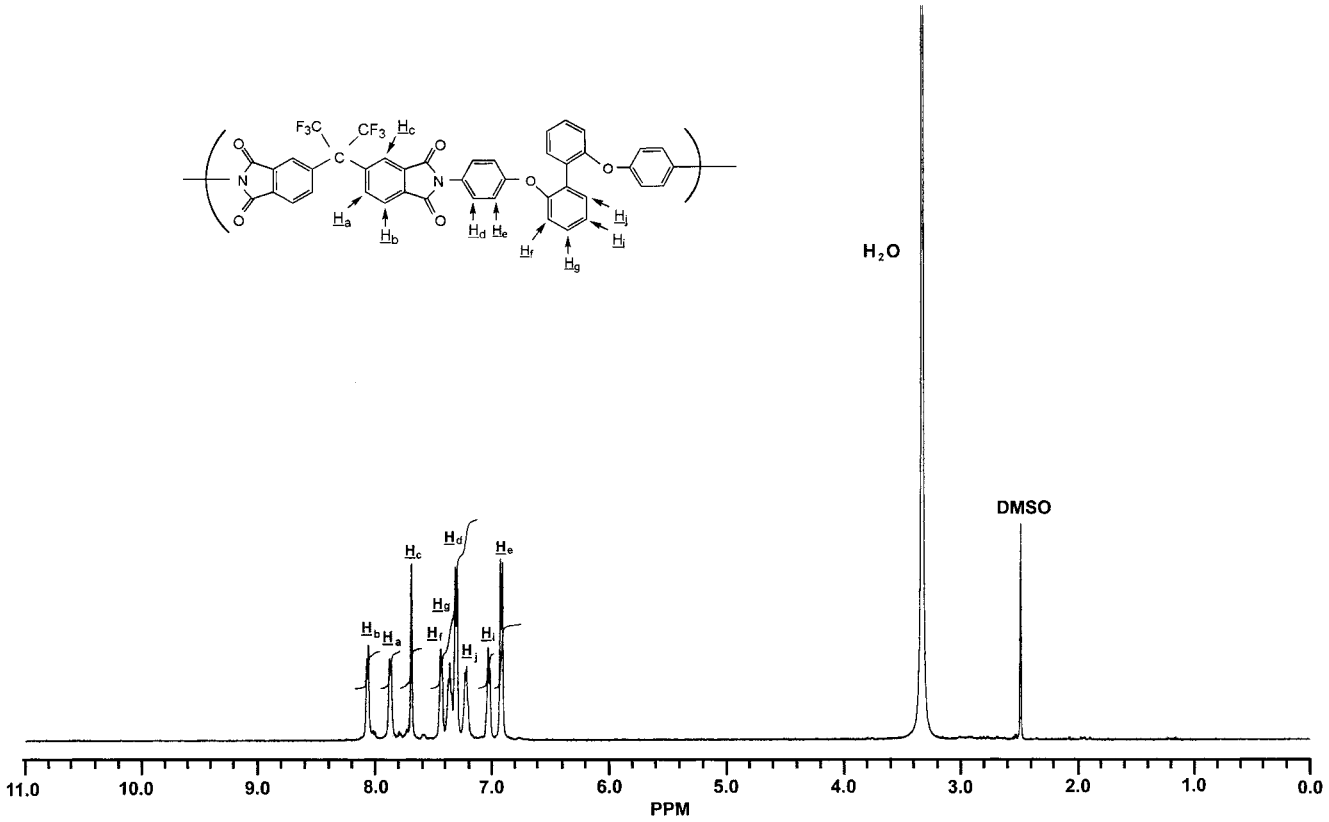

Figure 4. ^{1}H NMR spectrum of the soluble poly(ether imide) 6FPEI.

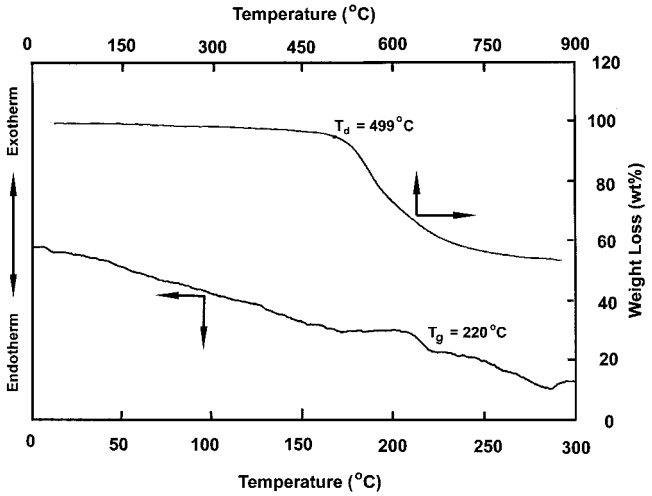

Figure 5. DSC and TGA thermograms of the pristine poly(ether imide) 6FPEI.

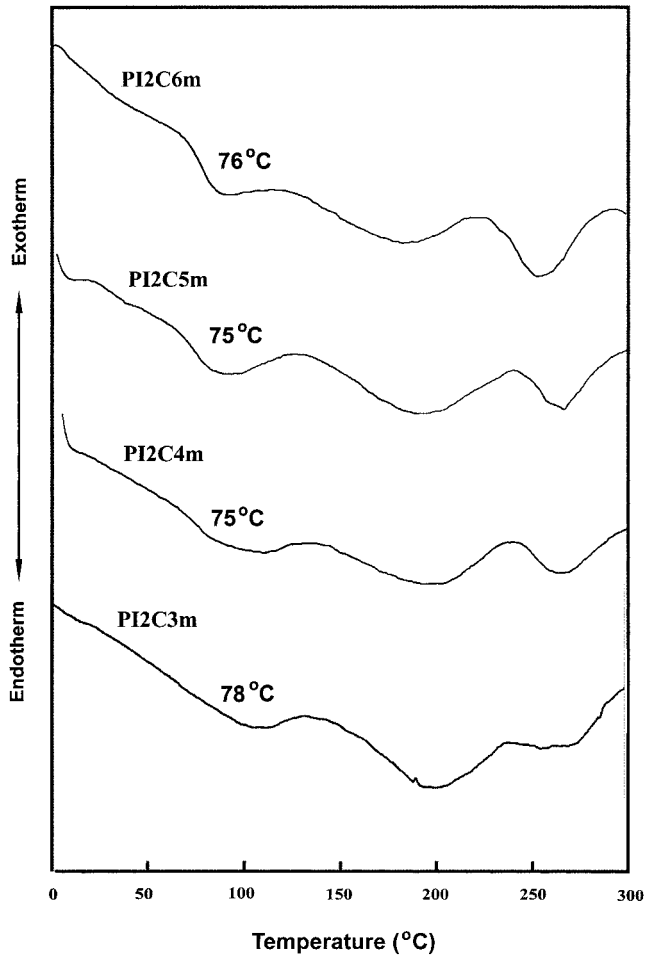

Figure 6. DSC thermograms of the NLO guest−host poly(ether imide).

section. This slow first-stage degradation behavior was not found in the pristine chromophores. This implies that polymer matrices play an important role in affecting the degradation behavior of the NLO-active guest−host system. The interaction among the chromophores decreases as the chromophores are doped into polymer matrices. This makes chromophores more susceptible to sublime at high temperatures. Moreover, the first-stage thermal degradation temperature decreases as the chromophore content increases. The plasticizer effect

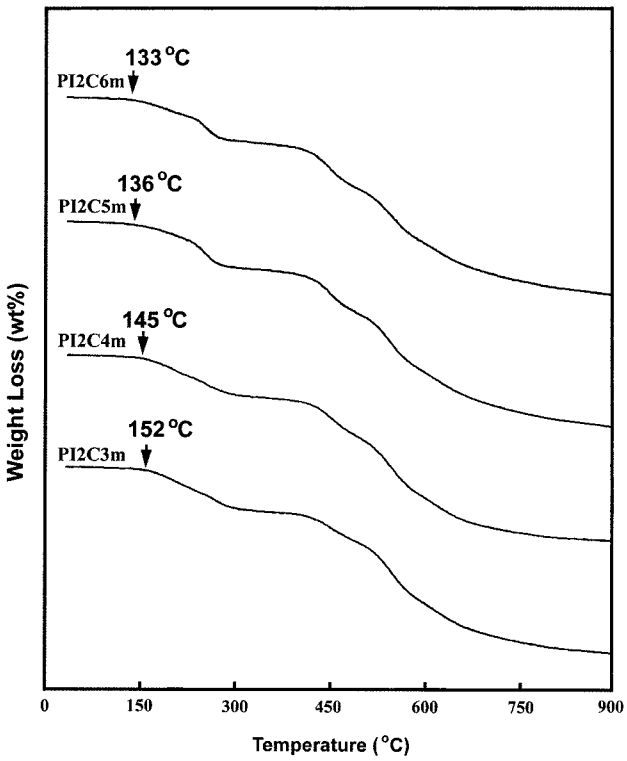

Figure 7. TGA thermograms of the NLO guest−host poly(ether imide).

becomes more pronounced as the doping level increases. This leads to easier sublimation of the chromophores.

Optimization of the Poling Condition. To optimize the poling temperature and investigate the sublimation of the chromophore in the guest−host systems, a UV−vis spectrophotometer was utilized to trace the chromophores in polymer host. Figure 8 shows the absorption characteristic of the NLO-active poly(ether imide)s thermal-treated at various temperatures for 1 h, respectively. No detectable decay of UV intensity was observed after thermal treatment at 170 °C for 50 h. However, a sharp decrease of the absorbance was observed when temperatures were higher than 170 °C. This temperature is slightly higher than the thermal degradation temperatures observed in DSC and TGA thermograms for guest−host samples. This result indicates that the endothermic peak observed in DSC thermogram and the first-stage degradation in TGA thermogram are caused by the sublimation of chromophores. Similar phenomena have been observed in other literature.[34−35] However, thermal treatments experiment and thermal analysis seem not to provide enough information for optimizing poling condition. In general, the SH signal seems to reach a maximum when the poling temperature approaches the glass transition temperature. However, maximum SH signals were found at ca. 150 °C for the NLO-active guest−host system in this work. This evidences that the lowest thermal transitions (70−80 °C) found in DSC thermograms is not a glass transition temperature of the NLO-active guest−host poly(ether imide). Maximum orientation of the chromophores in the polymer matrices is not achievable at this transition temperature.

On the basis of the above, an optimized poling/curing process was chosen as follows: the polymer films were heated to 120 °C. And then electric field was switched on. The sample was poled from 120 to 150 °C at a rate

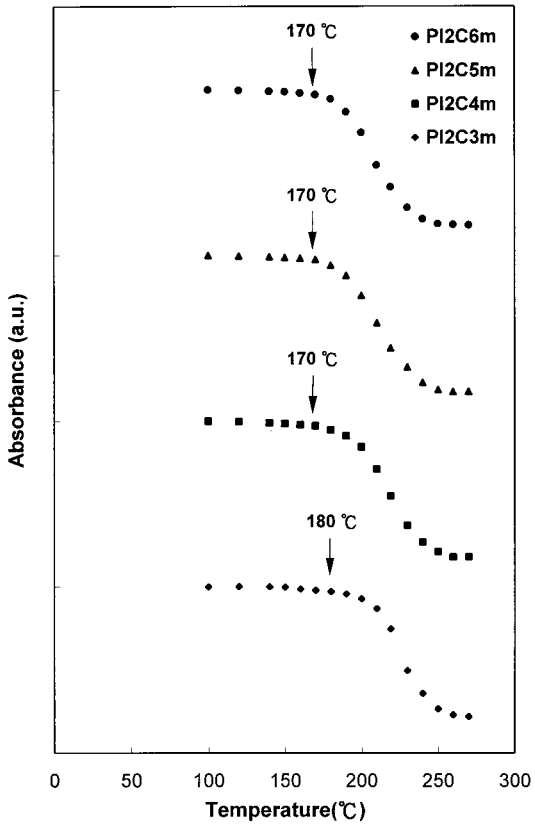

Figure 8. Thermal stability of the NLO guest−host poly(ether imide) measured by a UV−vis spectophotometer.

of 10 °C/h. Finally, the poled polymeric film was cooled to room temperature in the presence of an electric field.

Dielectric Analysis. Dielectric spectroscopy is a useful technique for investigating the thermal relaxation behavior of NLO systems because of its high sensitivity to reorientation of the permanent dipole. Parts a and b of Figure 9 show the temperature dependence of the dielectric constant and dielectric loss tangent for the pristine poly(ether imide) 6FPEI. In the dielectric constant spectrum (Figure 9a), two relaxation modes, which were assigned as α- and β-relaxations, were found. The α-relaxation corresponding to the glass transition of the poly(ether imide) was observed from 150 to 250 °C. The β-relaxation associated with the rotational motion of the biphenyl ether was located from 50 to 150 °C. In addition to these relaxation modes, a low oscillation strength assigned as γ-relaxation was found at dielectric loss tangent from −100 to +50 °C. The γ-relaxation may be contributed by the local motion of the trifluoromethyl group. Normally rigid polymer backbones would restrict motion of the trifluoromethyl group. This causes the trifluoromethyl group to possess a low oscillation strength despite having a strong dipole moment. These relaxation modes and their corresponding structural motions are shown in Scheme 3.

Parts a and b of Figure 10 show the temperature dependence of the dielectric constant and loss tangent, respectively, for the NLO-active guest−host sample PICz3m. In the dielectric constant spectrum (Figure 10a), an outstanding α-relaxation was observed from 85 to 180 °C. In the dielectric loss tangent spectrum (Figure 10b), three local motions were found in addition to the α-relaxation. Compared with the dielectric spectra of the pristine poly(ether imide), the α-and β-peaks for the guest−host PICz3m shift to lower temperatures and

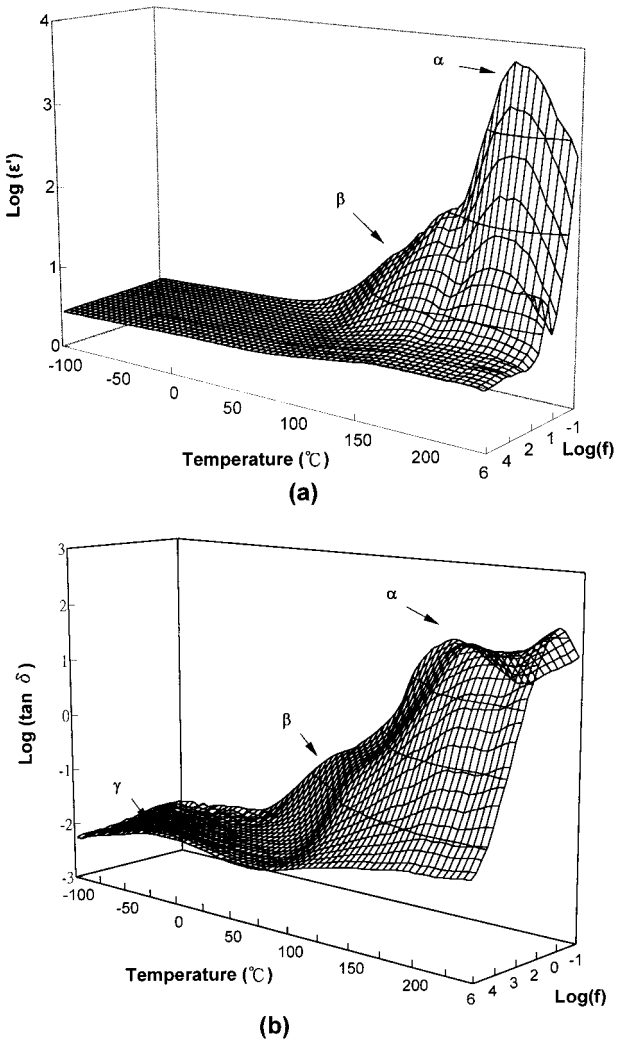

Figure 9. Dielectric spectra of the pristine poly(ether imide): (a) temperature and frequency dependence of the dielectric constant; (b) temperature and frequency dependence of the tangent δ.

coalesce at high frequencies. The transition observed in DSC thermogram is located in the temperature range of β-relaxation. This indicates that plasticizer effect of the chromophores make the biphenoxy group more mobile in NLO-active guest−host systems as compared to the pristine poly(ether imide). Similar behavior was found in the DSC thermograms. In Figure 6, the transition intensity, which contributed from local motion of the biphenoxy group, is increased with increasing chromophore content. For PICz3m, a weak σ-relaxation was observed from −50 to +40 °C, which corresponds to the local motion (i.e., crankshaft motion) of the aliphatic chain in the N-substituted position of carbazole.

Morphological Analysis. After poling, the polymeric films possess excellent optical transparency even though the chromophore content is up to 38 wt % (PICz6m). To further investigate the compatibility between the chromophores and poly(ether imide), a high-resolution scanning electron micrograph technique was applied. Figure 11 shows the scanning electron micrographs (40K×) of the guest−host polymers. Homogeneous fractured surfaces without apparent domains were observed in these polymeric films. This corroborates the excellent compatibility between the poly(ether imide) 6FPEI and the chromophore.

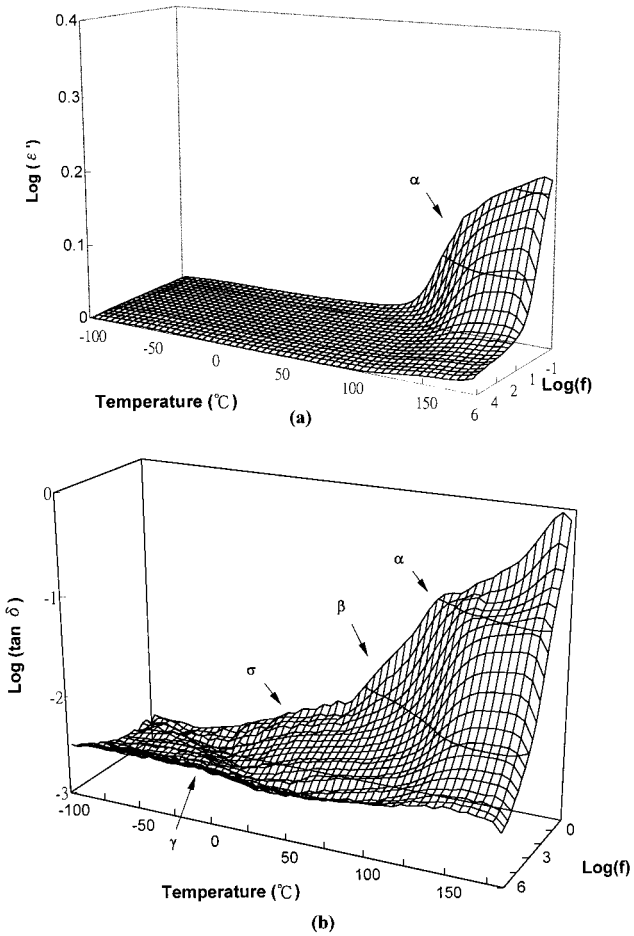

Figure 10. Dielectric spectra of the NLO poly(ether imide) PICz3m: (a) temperature and frequency dependence of the dielectric constant; (b) temperature and frequency dependence of the tangent δ.

Scheme 3. Various Relaxation Modes

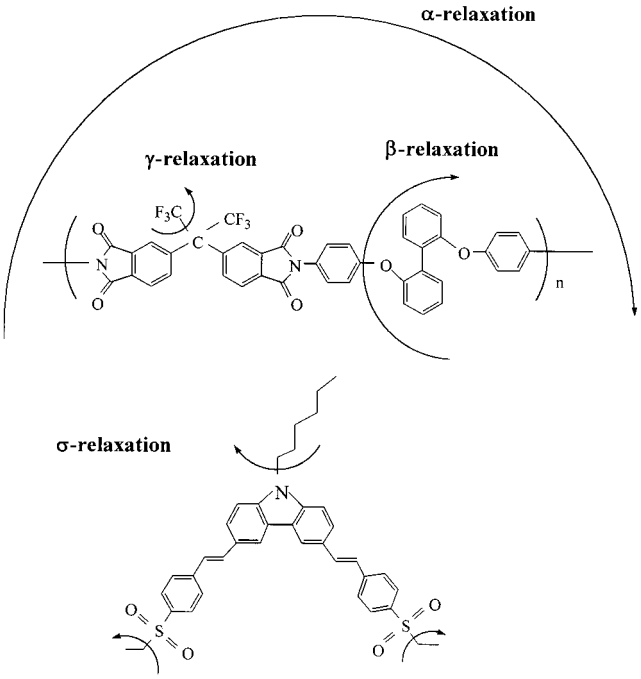

To further study the dispersion of the chromophore $Cz2PhSO_2$ in the poly(ether imide) matrices, an extraction experiment was performed. A cosolvent of acetonitrile and methanol was used to avoid collapse of the polymer. Figure 12 shows the scanning electron micrographs (7K×) of the solvent-treated polymers. The micrographs show droplets (dark section) left in the poly(ether imide) matrices (gray section) after solvent extraction. The droplets may be contributed from dissolution of the chromophores. Compared with untreated films, large size droplets were found in the SEM photographs for the solvent-treated films. Moreover, a significant increase in size for the droplets was observed as the chromophore content increased. No phase separation was found in the guest−host systems for DSC and DEA analysis. This implies that broad polydispersity of poly(ether imide) maybe plays an important role in enhancing compatibility. Fleer et al.[36,37] examined the molecular weight effect of polymers on interface. They concluded that the shorter chains tend to be in contact with the fillers if the molecular weight distribution is broad. To further investigate the dispersion of the poly(ether imide) in this aspect, the extracted film and extractant of the sample PICz3m were analyzed via GPC. High molecular weight M_w of 41 000 with a polydispersity index of 1.6 was observed for the extracted film. Low molecular weight M_w of 3400 with a polydispersity of 4.0 was observed for the extractant. This means the low molecular weight part of poly(ether imide) along with chromophores were extracted and the extracted sites were swollen during solvent treatment. More low molecular weight poly(ether imide) was extracted as the doping level increased. This is due to the fact that the chances of shorter chains in contact with the fillers are much greater. As a result of that, the droplet sizes in SEM photograph became larger.

Scheme 4 shows the schematic of the chromophores dispersing in poly(ether imide) matrices. In the schematic, as the chromophores are dispersed in the polymer matrices, two different domains are formed. Chromophore-rich (dispersed phase) and polymer-rich domains (continuous phase) are observed. In the polymer-rich domain, higher molecular weight poly(ether imide) is dominant for the polymer matrices. The chromophores present in the polymer-rich domains are constrained by the poly(ether imide). They cannot be dissolved during extraction process. In the chromophore-rich domains, not only the chromophores are dissolved, but part of the lower molecular weight poly(ether imide) as well. Blur interface may form owing to the compatibility between high molecular weight and low molecular weight poly(ether imide). The blur interfaces lead an excellent compatibility between the chromophores and poly(ether imide) matrix.[38]

Linear and Nonlinear Optical Properties. UV−vis absorption spectra of the PICz6m polymeric film before and after poling are shown in Figure 13. The maximum absorption wavelength (λ_{max}) of PICz6m polymer appears at 393 nm due to $\pi-\pi^*$ transition of the stilbene chromophore. It is noteworthy that no absorption was found at 532 nm. Figure 14 shows SH coefficients as a function of chromophore contents. The d_{33} and d_{31} values for the guest−host system PICzs range from 5 to 22 pm/V and from 2 to 5 pm/V, respectively. These SH coefficients increase essentially linearly as increasing chromophore content. This implies that no aggregation of chromophores is present at such a doping level of 38 wt %. Moreover, this further confirms that excellent compatibility is present between poly(ether imide) matrices and chromophores.

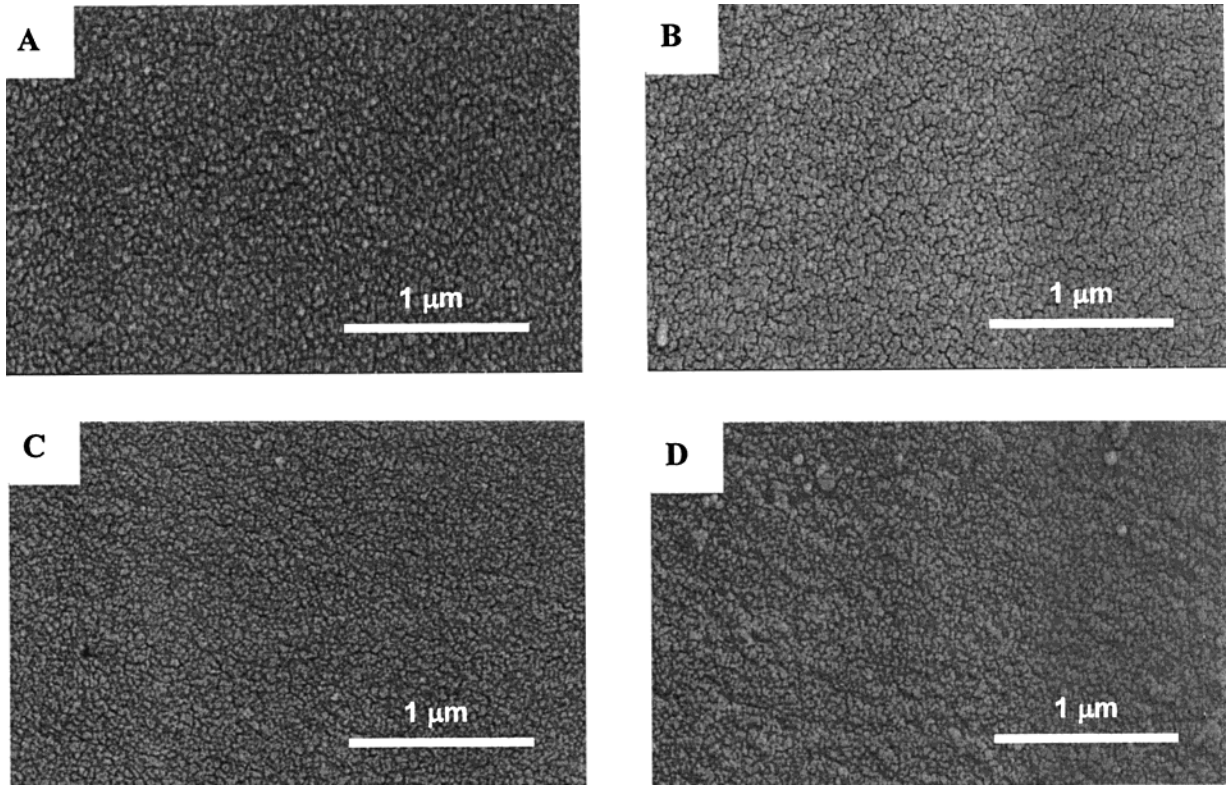

Figure 11. SEM photographs of the guest−host poly(ether imide)s (A) PICz3m, (B) PICz4m, (C) PICz5m, and (D) PICz6m.

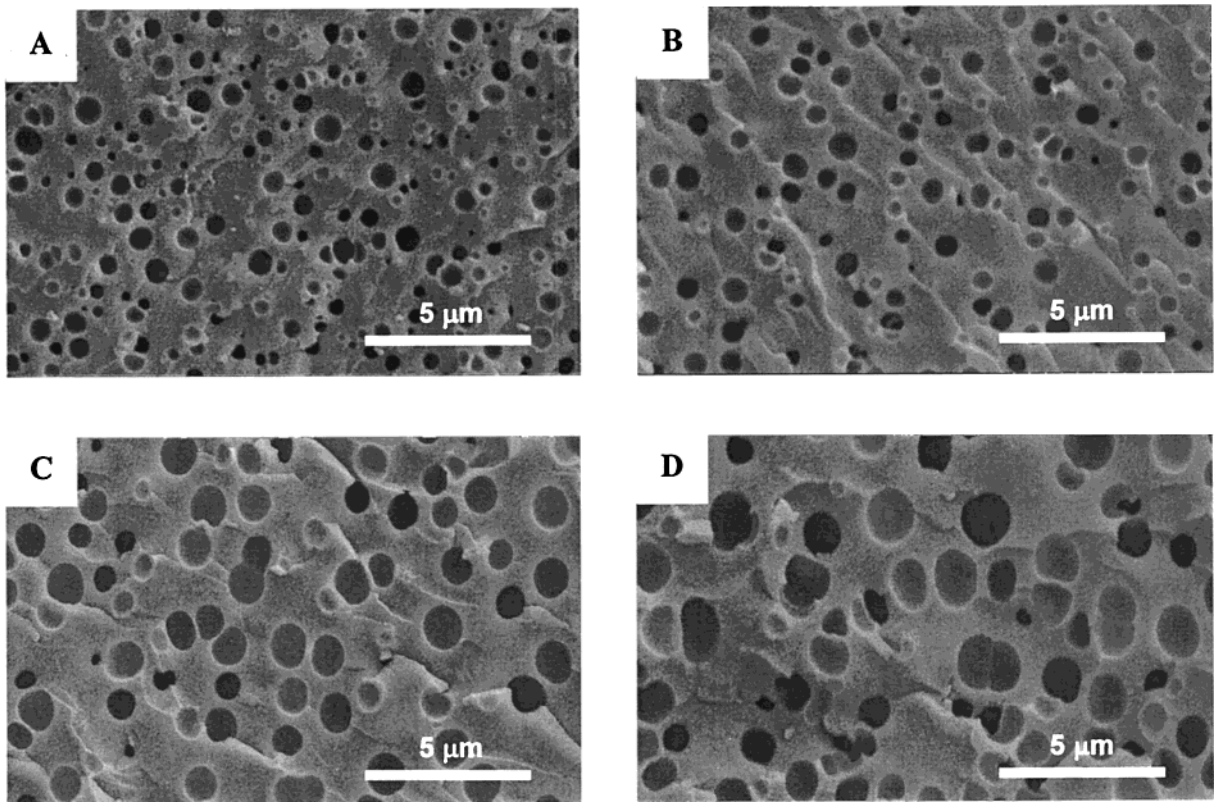

Figure 12. SEM photographs of the NLO poly(ether imide)s after solvent treatment: (A) PICz3m, (B) PICz4m, (C) PICz5m, and (D) PICz6m.

Thermal Dynamic Behavior. The temperature dependence of the dipole reorientation of the NLO polymer can be observed via measuring effective SH coefficient as a function of temperature. The effect of thermal treatment on the temporal stability was investigated by measuring the effective SH coefficient, $d_{eff}(t)/d_{eff}(0)$, at a heating rate of 1.2 °C/min. In general, the effective SH coefficient for a linear NLO polymer is stable at low temperatures but decays significantly at a specific temperature. The specific temperature is defined as effective relaxation temperature, T_0.[39] The T_0 value provides information on maximum device

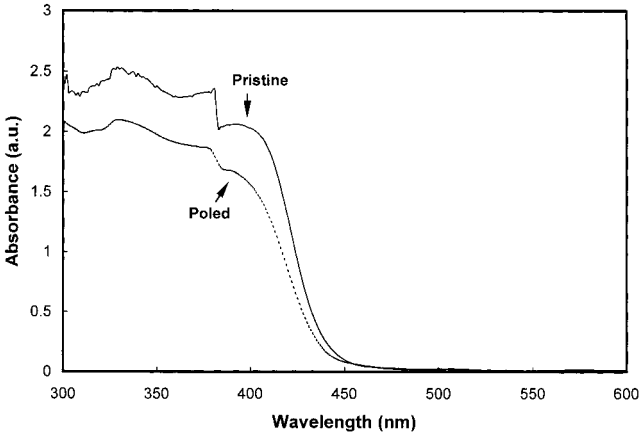

Figure 13. UV−vis spectra of the polymer PICz6m before and after poling process.

Scheme 4. Schematic Diagram of the Morphology in the Facture Surface for (a) the Polymer-Rich Domain and (b) the Chromophore-Rich Domain

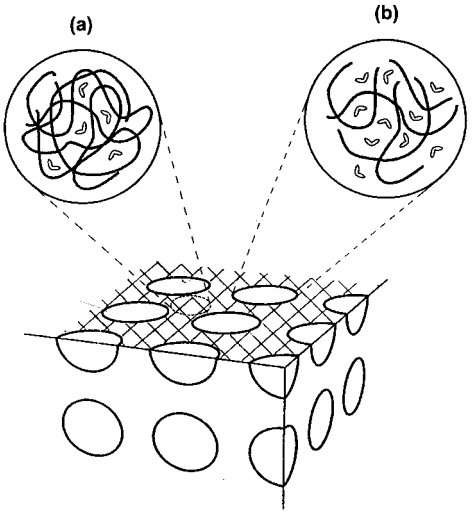

operating temperature that the film can endure, and allows quick evaluation of the temporal and thermal stability of the materials.

Figure 15 shows dynamic thermal stability of the NLO poly(ether imide) PICzs. SH signals were stable at low temperatures, and then fast decay was observed at temperatures higher than 90 °C. By extrapolatiom of slow and fast effective SH reorientation data, the T_0 value was found. Plasticization of chromophores plays an important role for the SH dynamic relaxation behavior. The T_0 value of the NLO-active PICz3m corresponds to the α-relaxation observed from DEA. Plasticization of the chromophores plays an important role in affecting T_0 values. The T_0 values are decreased with increasing chromophore content. It is noteworthy that the T_0 values observed from SH signal dynamic behavior are higher than thermal transition temperatures from DSC thermogram. Chromophore size and thermal aging during the poling procedure are also the important factors affecting T_0 values. The literature[40−43] indicate that isothermal physical aging under sub-T_g depresses the size and distribution of local free volumes. In this work, thermal annealing was performed during poling process. Moreover, two-dimensional chromophores possess a larger rotational radius than one-dimensional ones because of their bending structures.

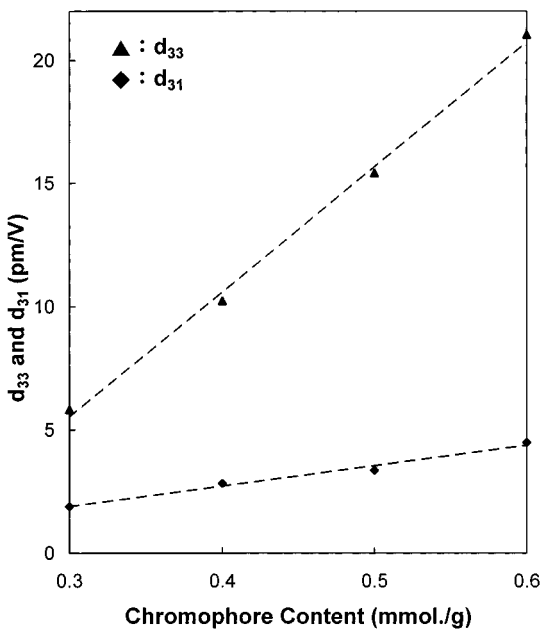

Figure 14. d_{33} (▲) and d_{31} (◆) values as a function of chromophore content per grams of poly(ether imide).

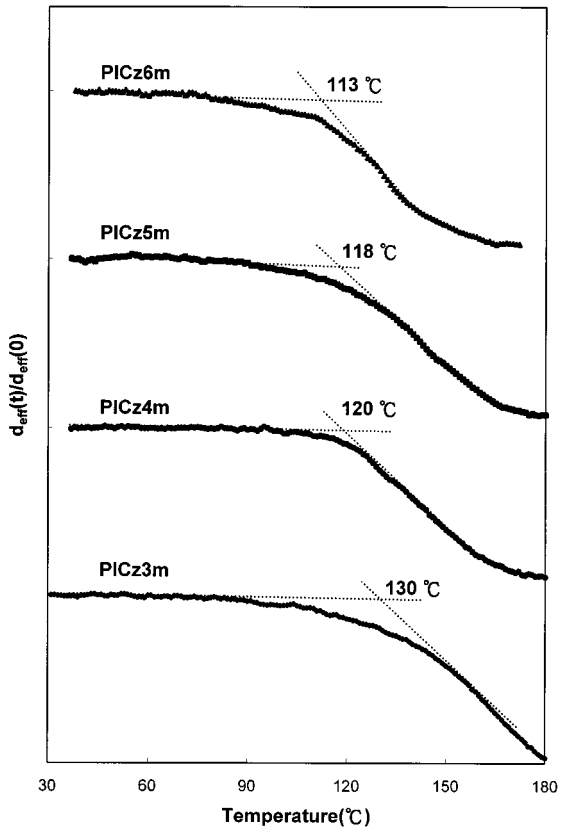

Figure 15. Temperature dependence of the dipole reorientational dynamics of the NLO guest−host polymers.

Lackritz et al.[44] developed a rotational Brownian motion model to explain reorientation of chromophores in polymer matrices. In Scheme 5, this model is utilized to analyze the reorientation of one-dimensional chromophore and two-dimensional chromophores in polymer matrices, respectively. In Scheme 5a, the one-dimensional chromophore would rotate around its geometrical center. The dipole moment, μ, is along the major geometrical axis of the chromophore. In the case, the rotational volume can be the sum of two cones. In

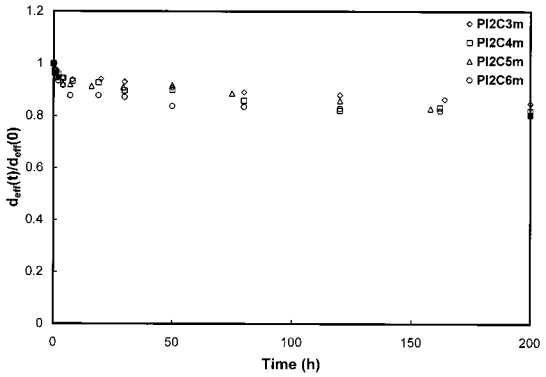

Figure 16. Time dependence of the dipole reorientation of the NLO polymers (◇) PICz3m, (□) PICz4m, (△) PICz5m, and (○) PICz6m at 60 °C.

Scheme 5. Schematic Diagram Shows (a) a One-Dimensional and (b) a Two-Dimensional Chromophore Rotating in the Polymer Matrix, Where μ Is the Dipole Moment, l Is the Axial Length of the Chromophore, r Is the Radius of the Cross Section of the Chromophore, and θ_0 Is the True Wedge Angle of the Chromophore Scanning

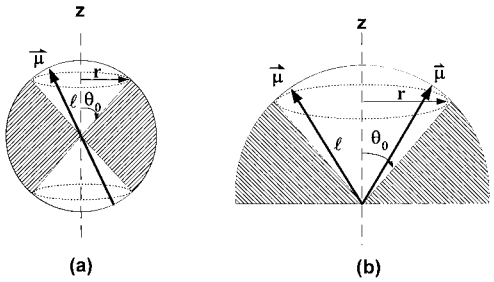

Scheme 5b, the two-dimensional chromophore can be visualized as the one wobbling around the joint end and rotating within one corn. The net dipole moment is normalized to the direction of the two charge transfers. As a result, the rotational cone volume of two-dimensional chromophore is much larger than that of one-dimensional chromophore. This large rotational volume retards the randomization of the oriented two-dimensional chromophores in polymer matrices.

Temporal Relaxation Behavior. To investigate the long-term NLO stability of the guest−host systems, dipole reorientation of the aligned chromophore was detected as a function of time. After the optimized poling process, dipole reorientation of the oriented chromophores in the poly(ether imide) matrices was observed by measuring ratios of effective SH coefficients ($d_{eff}(t)/d_{eff}(0)$) at various temperatures for a certain period of time.

Figures 16 and 17 show the time-dependent decay of effective SH coefficient of the NLO guest−host systems. In Figure 16, the effective SH coefficient of the PICzs retained 80−90% of its original value at 60 °C for 200 h. A fast decay of the effective SH coefficent was observed at the beginning of the thermal treatment, and then the effective SH coefficent remained almost constant. As the temperature was elevated to 80 °C (Figure 17), a conspicuous decrease for the temporal stability was found. This phenomenon can be explained by molecular motion from DEA study mentioned in previous section. Local motion (i.e., crankshaft motion) of the aliphatic chain of the chromophore dominates decay of SH signal when the operating temperature is set at 60 °C. The relaxation of oriented chromophores is confined

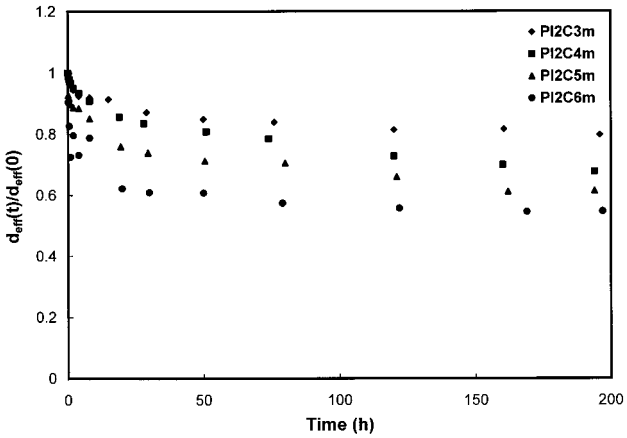

Figure 17. Time dependence of the dipole reorientation of the NLO polymers (◆) PICz3m, (■) PICz4m, (▲) PICz5m, and (●) PICz6m at 80 °C.

by the polymer backbone. When the operation temperature is elevated to 80 °C, the rotational motion of the biphenoxy groups would certainly randomize the oriented dipoles.

It is important to note that the SH signal is stable at the operating temperatures so close to the temperature range of α-relaxation. Thermal aging possibly contributed to the stabilization of SH signals. More importantly, the structural architecture of the chromophore has greater effect on the temporal stability. Two-dimensional chromophore requires larger rotational cone volume than one-dimensional one. Short-range relaxation such as crankshaft motion cannot provide enough local free volume to randomize the oriented dipoles. As a result, the effective SH coefficient only decays slightly at this temperature range. As the temperature elevates, long-range relaxation such as biphenoxy segment motion is allowed to occur. That provides enough local free volume to orient the poled chromophores. Moreover, the local free volume can be enlarged as the chromophore content is increased (i.e., greater plasticizer's effect). Yet, local free volume surrounding each chromophore was further decreased during an extended poling process.[45] The decrease in the local free volume restricts the dipole reorientation of the chromophore, and induces better temporal stability despite the operating temperatures are as high as 80 °C. Similar physical aging effect on temporal stability of NLO polymers was also observed in the literature.[46−48] These results imply that the rotational volume of the chromophore $Cz2PhSO_2$ is very close to the free volume of the polymer matrices when the operating temperature is close to T_g. This is in contrast to fast decay of the oriented dipoles of other NLO guest−host systems at temperatures close to T_g.[49−52]

Conclusion

In this work, a two-dimensional chromophore with sulfonyl groups and an organosoluble poly(ether imide) were synthesized. By doping of the chromophores into poly(ether imide), an NLO guest−host system was obtained. This guest−host system possesses excellent compatibility even though the chromophore content is as high as 38 wt %. Their second harmonic coefficients, d_{33} are in the range of 5−22 pm/V. In addition to the interaction between chromophores and poly(ether imide), the wide molecular weight distribution of the poly(ether imide) plays an important role in promoting the

compatibility. A significant feature to enhance the compatibility in the guest−host systems is the presence of blur interface. An apparent structural effect on the thermal stability was observed for the two-dimensional chromophore. This two-dimensional chromophore has a large molecular size, which corresponds to the free volume of the poly(ether imide) during glass transition. The effect of two-dimensional structure makes the guest−host system possessing excellent temporal stability despite that the operating temperature is close to glass transition range.

Acknowledgment. The authors thank the National Science Council of Republic of China for financial support of this work (Grant NSC88-2216-E-007-009).

References and Notes

(1) Prasad, P. N.; Williams, D. J. *Introduction to Nonlinear Optical Effects in Molecules and Polymers*; John Wiley: New York, 1991.
(2) Lindsay, G. A.; Singer, K. D. *Polymers for Second-Order Nonlinear Optics;* American Chemical Society: Washington, DC, 1995.
(3) Jenekhe, S. A.; Wynne, K. J. *Photonic and Optoelectronic Polymers*; American Chemical Society: Washington, DC, 1995.
(4) Li, F.; Kim, K. H.; Kulig, J. J.; Savitski, E. P.; Brittain, W. J.; Harris, F. W.; Cheng, S. Z. D.; Hubbard, S. F.; Singer, K. D. *J. Mater. Chem.* **1995**, *5*, 253.
(5) Nemoto, N.; Miyata, F.; Nagase, Y.; Abe, J.; Hasegawa, M.; Shirai, Y. *Macromolecules* **1996**, *29*, 2365.
(6) Miller, R. D.; Burland, D. M.; Jurich, M.; Lee, V. Y.; Moylan, C. R.; Thackara, J. I.; Twieg, R. J.; Verbiest, T.; Volksen, W. *Macromolecules* **1995**, *28*, 4970.
(7) Lindsay, G. A.; Stenger-Smith, J. D.; Henry, R. A.; Hoover, J. M.; Nissan, R. A. *Macromolecules* **1992**, *25*, 6075.
(8) Chen, L. T.; Tam, W.; Marder, S. R.; Stiegman, A. E.; Rikken, G.; Spangler, C. W. *J. Phys. Chem.* **1991**, *95*, 10631.
(9) Chen, L. T.; Tam, W.; Marder, S. R.; Stiegman, A. E.; Rikken, G.; Spangler, C. W. *J. Phys. Chem.* **1991**, *95*, 10643.
(10) Yamamoto, H.; Katogi, S.; Watanabe, T.; Sato, H.; Miyata, S.; Hosomi, T. *Appl. Phys. Lett.* **1992**, *60*, 935.
(11) Zyss, J.; Oudar, L. L. *Phys. Rev. A* **1982**, *26*, 2016 and 2018.
(12) Miyata, S.; Sasabe, H. *Poled Polymers and Their Applications to SHG and EO Devices*; Gordon and Breach Science: Australia, 1997.
(13) Kippelen, B.; Tamura, K.; Peyghambrian, N.; Padias, A. B.; Hall, H. K. *J. Phys. Rev.* **1993**, *B48*, 10710.
(14) Peng, Z.; Bao, Z.; Yu, L. *J. Am. Chem. Soc.* **1994**, *116*, 6003.
(15) Zhang, Y.; Ghosal, S.; Casstevens, M. K.; Burzyaski, R. *Appl. Phys. Lett.* **1994**, *66*, 2561.
(16) Hoegl, H. *J. Phys. Chem.* **1965**, *69*, 755.
(17) Wada, T.; Zhang, Y. D.; Yamakado, M.; Sasabe, H. *Mol. Cryst. Liq. Cryst.* **1993**, *277*, 85.
(18) Wada, T.; Zhang, Y. D.; Choi, Y. S.; Sasabe, H. *J. Phys. D: Appl. Phys.* **1993**, *26*, B221.
(19) Nalwa, H. S.; Watanabe, T.; Miyata, S. *Adv. Mater.* **1995**, *7*, 754.
(20) Singer, K. D.; Kuzyk, M. G.; Sohn, J. E. *J. Opt. Am. B* **1987**, *4*, 968.
(21) Hampsch, H. L.; Yang, J.; Wong, G. K.; Torkelson, J. M. *Macromolecules* **1990**, *23*, 3640.
(22) Firestone, M. A.; Ratner, M. A.; Marks, T. J. *Macromolecules* **1995**, *28*, 6296.
(23) Boyd, G. T.; Francis, C. V.; Trend, J. E.; Ender, D. A. *J. Opt. Am. B* **1991**, *8*, 887.
(24) Bell, V. L.; Stump, B. L.; Gager, H. *J. Polym. Sci. Polym. Chem. Ed.* **1976**, *14*, 2275.
(25) Takekoshi, T.; Wirth, J. G.; Heath, D. R.; Kochanocoski, J. E.; Manello, J. S.; Webber, M. T. *J. Polym. Sci., Polym. Chem. Ed.* **1980**, *18*, 3069.
(26) Feld, W. A.; Ramalingam, B.; Harris, F. W. *J. Polym. Sci. Polym. Chem. Ed.* **1983**, *21*, 319.
(27) Ghatge, N. D.; Shinde, B. M.; Mulik, U. P. *J. Polym. Sci. Polym. Chem. Ed.* **1984**, *22*, 3359.
(28) Imai, Y.; Maldar, N. N.; Kakimoto, M. *J. Polym. Sci. Polym. Chem. Ed.* **1984**, *22*, 2189.
(29) Jeong, H. J.; Oishi, Y.; Kakimoto, M.; Imai, Y. *J. Polym. Sci. Polym. Chem. Ed.* **1991**, *29*, 39.
(30) Qi, Y.; Wang, Z. Y. *Macromolecules* **1996**, *29*, 792.
(31) The T_d values of the commercial azo dyes DO3 and DR19 were observed by measuring the onset temperature of the exothermic peak using Seiko SSC/5200 differential scanning calorimeter and detecting 5 wt % weight loss using Seiko 2200 thermogravimetric analyzer.
(32) Singer, K. D.; King, L. A. *J. Appl. Phys.* **1991**, *70*, 3251.
(33) Wong, K. Y.; Jen, A. K. Y. *J. Appl. Phys.* **1994**, *75*, 3308.
(34) Shu, Y. C.; Gong, Z. H.; Shu, C. F.; Breitung, E. M.; McMahon, R. J.; Lee, G. H.; Jen, A. K. Y. *Chem. Mater.* **1999**, *11*, 1628.
(35) Pauley, M. A.; Guan, H. W.; Wang, C. H. *J. Chem. Phys.* **1996**, *104*, 6834.
(36) Fleer, G. J.; Cohen Stuart, M. A.; Scheutjens, J. M. H. M.; Cosgrove, T.; Vincent, B. *Polymers at Interfaces*; Chapman & Hall: London, 1993.
(37) Sperling, L. H. *Polymeric Multicomponent Materials: an Introduction*; John Wiley & Sons: New York, 1997.
(38) Jones, R. A. L.; Richards, R. W. *Polymers at Surfaces and Interfaces*; Cambridge University Press: Cambridge, England, 1999.
(39) Tsutsumi, N.; Morishima, M.; Sakai, W. *Macromolecules* **1998**, *31*, 7764.
(40) HampSch, H. L.; Yang, J.; Wong, G. K.; Torkelsonm, J. M. *Polymer* **1989**, *30*, 40.
(41) Victor, J. G.; Torkelsonm, J. M. *Macromolecules* **1988**, *21*, 355.
(42) Lindsay, G. A.; Henry, R. A.; Hoover, J. M.; Knoesen, A.; Mortazavi, M. A. *Macromolecules* **1992**, *25*, 4888.
(43) Song, H. H.; Roe, R. J. *Macromolecules* **1987**, *20*, 2723.
(44) Liu, L. Y.; Ramkrishna, D.; Lackritz, H. S. *Macromolecules* **1994**, *27*, 5987.
(45) Goodson, T., III; Gong, S. S.; Wang, C. H. *Macromolecules* **1994**, *27*, 4278.
(46) Hampsch, H. L.; Yang, J.; Wong, G. K.; Torkelson, J. M. *Macromolecules* **1990**, *23*, 3648.
(47) Lee, S. C.; Kidoguchi, A.; Watanabe, T.; Yamamoto, H.; Hosomi, T.; Miyata, S. *Polym. J.* **1991**, *23*, 1209.
(48) Royl, J. S.; Torkelson, J. M. *Macromolecules* **1993**, *26*, 5331.
(49) Shi, Y.; Steier, W. H.; Chen, M.; Yu, L.; Dalton, L. R. *Appl. Phys. Lett.* **1992**, *60*, 2577.
(50) Walsh, C. A.; Burland, D. M.; Lee, V. Y.; Miller, R. D.; Smith, B. A.; Tweig, R. J.; Volksen, W. *Macromolecules* **1993**, *26*, 3720.
(51) Chen, J. I.; Marturunkakul, S.; Li, L.; Jeng, R. J.; Kumar, J.; Tripathy, S. K. *Macromolecules* **1993**, *26*, 7379.
(52) Tsutsumi, N.; Yoshizaki, S.; Sakai, W.; Kiyotsukuri *Macromolecules* **1995**, *28*, 6437.

MA0017485